Thermally Stable Ceramic-Based Nanocomposite Coatings for Versatile and Reusable Air Filtration Media

Original
Thermally Stable Ceramic-Based Nanocomposite Coatings
for Versatile and Reusable Air Filtration Media / Luceri, A., Perero, S., Cempura, G., Kruk, A., Ferraris, M., Balagna, Cristina.. - In: INTERNATIONAL JOURNAL OF APPLIED CERAMIC TECHNOLOGY. - ISSN 1744-7402. - 23:3(2026), pp. 1-15. [10.1111/ijac.70225]

Availability:
This version is available at: 11583/3013020 since: 2026-07-13T09:41:31Z

Publisher:
Wiley

Published
DOI:10.1111/ijac.70225

International Journal of Applied Ceramic Technology

The American Ceramic Society
ceramics.org

RESEARCH ARTICLE OPEN ACCESS

Thermally Stable Ceramic-Based Nanocomposite Coatings for Versatile and Reusable Air Filtration Media

Angelica Luceri[1] | Sergio Perero[1] | Grzegorz Cempura[2] | Adam Kruk[2] | Monica Ferraris[1] | Cristina Balagna[1]

[1]Department of Applied Science and Technology, Politecnico di Torino, Turin, Italy | [2]International Centre of Electron Microscopy for Materials Science, AGH University of Science and Technology, Kraków, Poland

Correspondence: Cristina Balagna (cristina.balagna@polito.it)

Received: 20 February 2026 | **Revised:** 25 May 2026 | **Accepted:** 1 June 2026

Keywords: antibacterial | ceramic composite coating | filters | silver | sputtering | virucidal

ABSTRACT

Reusable air filtration systems are increasingly explored as sustainable solutions for indoor air quality control, provided that effective sterilization and long-term antimicrobial performance can be guaranteed. This study investigates thin ceramic-based nanocomposite coatings applied to conventional air filter media to enable dry-heat sterilization and repeated reuse. Silver nanoclusters embedded in silica (SiO_2) or zirconia (ZrO_2) matrices were deposited by radio-frequency co-sputtering onto metallic, glass-fiber, and polymeric substrates. Thermally stable ceramic oxides were selected to preserve coating integrity, regulate silver ion release, and maintain the original filter porosity. Morphological and structural characterization (FESEM, TEM, UV–Vis, XRD) revealed porous amorphous SiO_2-based coatings and denser ZrO_2-based coatings, both featuring a uniform distribution of silver nanoclusters. Antibacterial and antifungal activity against *Staphylococcus epidermidis*, *Escherichia coli*, and *Candida albicans* was confirmed through inhibition halo tests, CFU quantification, and aerosol contamination experiments. A key outcome is the demonstrated thermal regenerability of the coated filters, which retained antimicrobial efficacy after multiple dry-heat sterilization cycles at 200°C. While silica-based coatings exhibited higher silver ion release, zirconia-based coatings provided improved release control and structural stability. These results highlight ceramic-based nanocomposite coatings as a promising approach for durable, regenerable, and scalable antimicrobial air filtration systems.

1 | Introduction

The progressive deterioration of air quality and the increasing presence of airborne biological contaminants represent major concerns for human health, particularly in indoor environments. Airborne bioaerosols can remain suspended for extended periods and penetrate deeply into the respiratory tract, contributing to respiratory diseases and facilitating the transmission of infectious agents. The recent COVID-19 pandemic has further emphasized the urgent need for effective air filtration systems capable of limiting the spread of airborne pathogens [1–5]. In parallel with health concerns, growing attention has been directed toward the environmental impact of disposable air filters. Conventional filtration systems are typically designed for single-use operation and require frequent replacement, resulting in significant material waste and associated environmental burdens. Reusable air filters represent a promising alternative; however, their widespread adoption is constrained by the lack of effective, robust sterilization strategies that do not compromise filtration efficiency or functional performance. In this context, ceramic materials and ceramic-based technologies offer distinctive advantages for advanced air filtration applications. While fully ceramic filter media have been widely investigated for demanding environments, including nuclear facilities and high-risk industrial settings, due to their excellent thermal stability, chemical inertness, and mechanical robustness [6–9]. These intrinsic properties allow ceramic systems to withstand high-temperature sterilization while preserving structural integrity and filtration performance, enabling long-term reuse. Moreover, ceramics have shown high efficiency in removing microorganisms in both water and air filtration applications [10–12]. More recently, porous ceramic-based bubble-enhanced air purification systems have exploited tunable pore architectures and gas–liquid interfaces to achieve strong $PM_{2.5}$ removal and simultaneous reduction of gaseous pollutants and microorganisms, further supporting the potential of porous ceramics for multifunctional, regenerable air cleaning systems [13]. However, the use of thin ceramic-based coatings represents an alternative and more versatile strategy, enabling the integration of ceramic functionalities onto conventional non-ceramic filter substrates. Thin functional ceramic coatings represent a versatile and scalable strategy to impart additional functionalities to conventional filtration substrates, such as antimicrobial activity, chemical resistance, and fouling control, while preserving the bulk structure, porosity, and pressure drop of the filter media [14, 15]. This approach is particularly attractive for retrofitting existing filtration systems and extending their durability and functional lifetime. For example, Zr–Ag co-doped TiO_2 thin films deposited on ceramic tiles have shown combined photocatalytic pollutant removal and antimicrobial activity against aerobic bacteria, highlighting the potential of functionalized ceramic systems for air-cleaning applications in confined environments [16]. To prevent bacterial proliferation on filters, especially under humid conditions and dust accumulation, silver incorporation into ceramic matrices has been widely investigated. Silver nanoparticles (AgNPs) exhibit broad-spectrum antibacterial and antifungal activity through multiple mechanisms [17] and can be immobilized within oxide networks or on porous ceramic surfaces. Silver-containing leucite glass ceramics have demonstrated strong antibacterial activity and improved mechanical performance, with CFU-based assays confirming effectiveness against *Staphylococcus aureus* and *Escherichia coli* [18]. Furthermore, studies on ion-exchanged antibacterial glazes have clarified the diffusion and controlled release of Ag^+ ions from ceramic surfaces, providing insight into long-term antimicrobial performance [19]. Similarly, Li_2O–ZrO_2–SiO_2 systems have shown intrinsic antibacterial properties, indicating that zirconia- and silica-based ceramic networks can stabilize silver species and enhance antimicrobial action [20]. Based on these studies, increasing attention is being devoted to thin and flexible ceramic composite coatings applicable to different air filtration media without affecting porosity, pressure drop, or mechanical integrity. Here, radio-frequency (RF) co-sputtering was used to develop flexible ceramic-based composite coatings, addressing reusability requirements [21, 22] and green approach considerations [23–27]. The patented and industrially scalable process enables versatile, substrate-compatible, and environmentally friendly deposition of nanoparticle-containing films [28, 29]. In this work, silica (SiO_2) and zirconia (ZrO_2) were selected as ceramic matrices due to their complementary physicochemical properties and relevance in applied ceramics. Using silica or zirconia as a matrix promotes homogeneous dispersion of silver nanoclusters and controlled ion diffusion, enhancing antimicrobial activity [30–35], providing high thermal stability and durability, and supporting silver-based systems under harsh conditions [34, 36]. Their comparison offers insight into the role of ceramic structure in regulating antimicrobial performance. Despite extensive research on antimicrobial air-filtration coatings, the thermal regenerability of such coatings remains largely unexplored. Most studies rely on mild or chemical sterilization routes that may compromise coating integrity, whereas high-temperature dry sterilization requires thermally stable materials. Therefore, this work develops Ag nanocluster-based antimicrobial coatings embedded in ceramic matrices, silica, and zirconia, and deposited on different air filtration substrates, with particular focus on maintaining antimicrobial activity after repeated thermal regeneration cycles at 200°C.

2 | Materials and Methods

2.1 | Co-Sputtering Deposition

The co-sputtering technique was employed to deposit two composite coatings made up of silver nanoclusters embedded within a silica or zirconia matrix, according to a patented process [37]. The substrates were stainless steel filters (referred to as *Met*, in the text), glass-fiber filters (referred to as *Glass*, in the text), and a polymeric membrane (referred to as *Memb*, in the text). During the coating deposition process, two targets were simultaneously used. One target was silica or zirconia, to deposit the matrix (Sigma-Aldrich 99.99% purity), while the other one was a silver target, to form nanoclusters (Franco Corradi S.r.l. 99.9% purity). These targets operated in two different modes: RF mode for oxide materials and direct current mode (DC) for metal. Due to the low deposition rate of the oxide materials, the power applied to the oxide matrix targets was higher (200 W for silica and 250 W for zirconia) than the power applied to the silver target (3 or 5 W). Each deposition lasted for 1 h under a pure argon atmosphere. The acronym for the coated substrates was formed by adding a suffix denoting the matrix and the power applied to the silver target to the substrate name. For example, "*Glass-ZrO2-Ag5*" indicates a glass-fiber filter coated with a composite coating of silver nanoclusters and zirconia, applying a power of 5 W to the silver target.

2.2 | Compositional, Morphological, and Structural Analysis

Energy Dispersive Spectroscopy (EDS, EDAX PV 9900TM) determined the atomic percentages of elements constituting the coatings, Si for silica matrix, Zr for zirconia matrix, and Ag for the silver nanoclusters. These values were compared with data obtained from analyzing uncoated substrates.

Both the morphological investigation of uncoated and coated substrates was performed through electron microscopy (FESEM, QUANTA INSPECT 200, Zeiss SUPRATM 40TM, and Merlin Gemini II of ZEISS). Detailed morphological and compositional evaluation of the coatings was achieved with a Transmission Electron Microscope (TEM, Titan Cubed G2 60–300, FEI), featuring a Schottky field emission electron gun (X-FEG) high brightness source and a monochromator. Samples were cross-sectioned via FIB milling prior to TEM analysis, and a platinum protective layer was deposited to preserve surface integrity. The corresponding EDS maps were acquired using Energy Dispersive X-Ray Spectroscopy (EDX) with a ChemiSTEM EDX system, which is based on four windowless Silicon Drift Detectors (Super X).

UV–Visible analysis (UV–Vis, Shimadzu, UV 2600) was used to control the silver nature of both coatings within a wavelength range of 700–200 nm, and X-ray diffractometry (XRD) determined the phases present in both composite coatings. To avoid interference from the filter materials, UV–Vis and XRD analyses were performed on soda-lime glass substrates used as model systems.

2.3 | Silver Ions Release Test in Water

The release of silver ions was assessed in water. Coated air filter samples (1 × 1 cm^2) were immersed in 30 mL of water at room temperature, with the coated surface faced up. The concentration of silver ions (in ppm) released into the water was measured after 3 h, 1, 3, 7, and 14 days using a spectrophotometer (Hanna Instruments TM). Data collected at each time point were statistically analyzed based on three samples

2.4 | Antimicrobial Tests With Antipathogenic Microorganisms

Both qualitatively and quantitatively antimicrobial tests were conducted to study the antibacterial behavior of the deposited coatings. This analysis included the inhibition halo test, the antimicrobial dilution test, and the bacterial contamination test, using a bacterial aerosol generator. The inhibition halo test involved placing uncoated and coated air filters (1 × 1 cm^2) on an agar in contact with the bacterial solution (McFarland index of 0.5) of *Staphylococcus epidermidis* (nonpathogenic Gram +, ATCC14990) or *E. coli* (nonpathogenic Gram −, ATCC8739), or *Candida albicans* (nonpathogenic fungal strain, ATCC10231), following the standard [38]. All samples used for halo inhibition tests were consistently prepared in 1 × 1 cm^2 dimensions to ensure comparable results. The formation of a bacteria-free halo around the samples after 24 h of incubation at 35°C indicated antibacterial or antifungal effects. The antimicrobial dilution test quantified bacterial colony-forming units (CFU), proliferated in a bacterial broth, which was inoculated with *S. epidermidis* (initial CFU number approximately 5×10^5 CFU/mL) [39]. Uncoated and one-sided coated air filters were analyzed with an exposed area of about 2 × 0.5 cm^2. After 24 h of incubation at 35°C, the bacterial broth was serially diluted with a physiological solution several times. The diluted solutions were spread on agar. The CFU growth after an incubation of 24 h at 35°C was counted. In addition, the CFU adhered on the sample surface was also quantified, after subjecting samples to vortexing in a physiological solution for 5 min. This vortexed solution was diluted and, as described previously for broths, spread on agar and incubated; at the end, the CFU was counted.

The third test aimed to simulate a ventilation system under a controlled and more severe bacterial contamination of the air filter surface. Air filters were contaminated using a generator of bacterial bioaerosol (TOPAS, ATM 220). The bacterial solution of *S. epidermidis* (McFarland index at 5) was nebulized on coated and uncoated air filters for 5, 10, and 30 min. The contaminated surface of the filter was put in contact with the Mueller Hinton agar plate and incubated at 35°C for 24 h. The growth of bacteria around and on samples was assessed. This test followed a protocol developed by the authors in the laboratory, already reported in [30], as there are not any standards specific for this analysis.

TABLE 1 | Atomic percentage of silicon, zirconium, and silver contained in the uncoated and coated air filters.

Substrate	Coating	%at. Si	Zr	Ag
Met	Uncoated	0.7 ± 0.1	—	—
	SiO2-Ag5	4.3 ± 0.1	—	2.7 ± 0.1
	ZrO2-Ag5	0.3 ± 0.4	2.7 ± 0.5	4.2 ± 0.6
Glass	Uncoated	10.1 ± 0.2	—	—
	SiO2-Ag5	12.0 ± 0.7	—	1.6 ± 0.03
	ZrO2-Ag5	12.1 ± 1.1	0.8 ± 0.1	1.2 ± 0.1
Memb	Uncoated	—	—	—
	SiO2-Ag3	1 ± 0.03	—	0.8 ± 0.03
	ZrO2-Ag5	—	0.8 ± 0.01	1.2 ± 0.2

To obtain a quantitative indication of the coatings effect, a CFU count test was conducted on the samples after 30 min of contamination. Contaminated samples were immersed in broths solution and incubated at 35°C for 24 h; then, the solutions were serially diluted and spread on agar plates, as previously described. In the discussion, a suffix "-cont" was added to the name when referring to contaminated samples.

2.5 | Thermal Treatment for Filter Regeneration

After contamination with an aerosol generator, filters were thermally treated at 200°C to achieve decontamination and regeneration. The metallic and glass-fiber-based filters underwent three cycles of heating and cooling up to 200°C with a dwell time of 10 min. At the end of the thermal treatment, to investigate the residual antibacterial effect of the coating after thermal regeneration, the samples were again contaminated with the bacterial bioaerosol, and the effect of coatings in inhibiting bacterial growth was examined both qualitatively, verifying colonies proliferated on the samples, and quantitatively, through the count of CFU test.

3 | Results and Discussion

3.1 | Compositional, Structural, and Morphological Characterization

This study compares silver nanocluster–ceramic composite coatings employing silica and zirconia as embedding matrices, deposited by RF co-sputtering on metallic, glass-fiber, and polymeric air filtration media. The central role of the ceramic matrix is to stabilize the silver nanoclusters, regulate their distribution, and preserve coating integrity under operational and regeneration conditions, while maintaining the intrinsic porosity of the filters. Table 1 reports the atomic percentages of Si, Zr, and Ag obtained by EDS analysis for uncoated and coated substrates. For all coated samples, the deposition process resulted in a clear increase in the

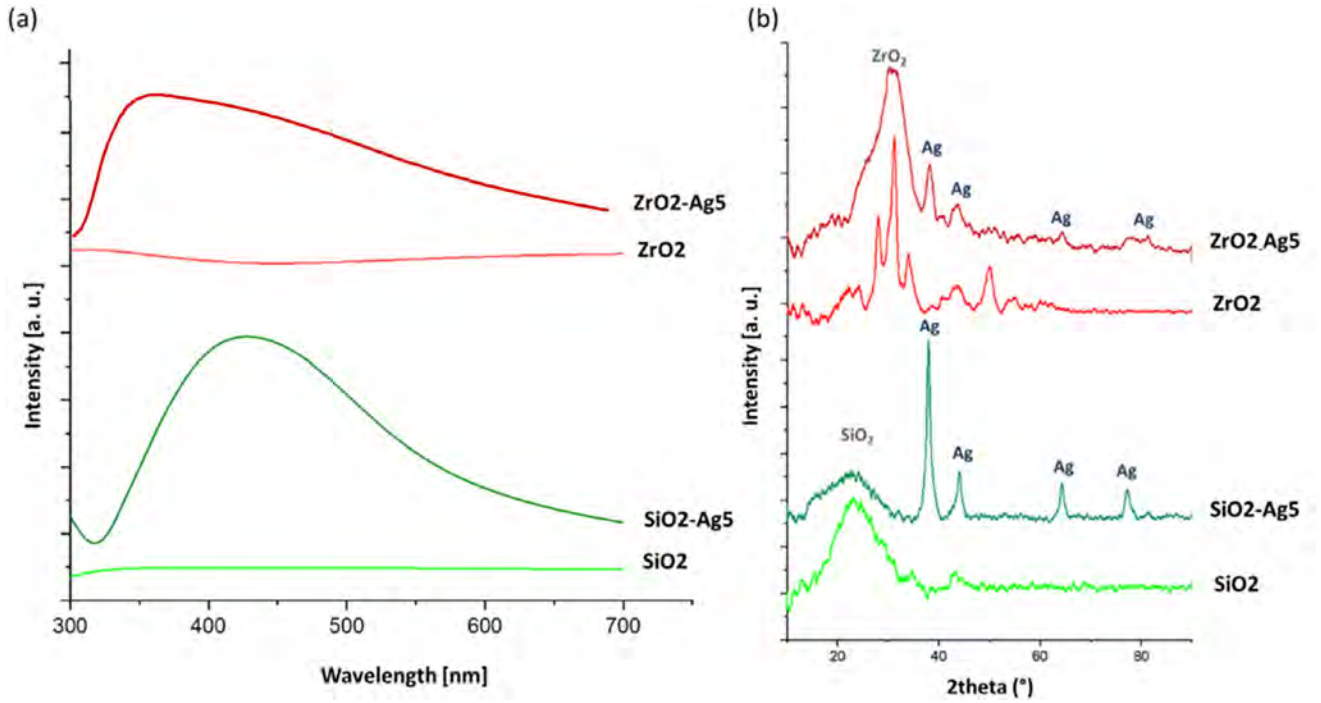

FIGURE 1 | UV–Vis (a) and XRD (b) patterns of SiO2, SiO2-Ag5, ZrO2, and ZrO2-Ag5 coatings deposited on soda-lime substrates.

content of Ag and of the corresponding ceramic matrix element (Si or Zr) compared with the uncoated substrates, confirming the successful formation of silver–ceramic composite coatings on the filtration media. The Ag target power was maintained at 5 W for metallic and glass-fiber filters, while it was reduced to 3 W for polymeric membranes to improve coating adhesion and homogeneity, as indicated by preliminary optimization trials. It is important to note that the measured compositions do not directly correspond to a fixed nominal target composition, as the co-sputtering process is governed by different sputtering yields and deposition rates of the involved materials. In particular, despite the higher power applied to the oxide targets (200–250 W), the effective incorporation of Si, Zr, and Ag is determined by their sputtering yield. This explains the relatively higher Ag content observed in some samples, especially on metallic substrates. Furthermore, substrate morphology and composition can influence the local deposition efficiency, contributing to the observed variability. It should be emphasized that the EDS analysis provides only semiquantitative compositional information for these systems. Due to the very limited coating thickness (~100 nm), the rough and porous morphology of the filtration substrates, and the possible contribution of the underlying substrate to the detected signal, the measured atomic percentages do not directly correspond to the actual volumetric composition of the deposited coatings. Therefore, the relatively high Ag values observed in some samples should not be interpreted as evidence of a silver-rich continuous phase, but rather as an effect of the combined influence of sputtering yield differences, local morphology, signal penetration depth, and substrate-related contributions during EDS acquisition.

In this work, the co-sputtering process was not aimed at achieving a predefined stoichiometric target composition. Instead, the deposition parameters were optimized to obtain homogeneous and adherent coatings with well-dispersed Ag nanoclusters and effective antimicrobial performance. The Ag–ceramic nanocomposite structure is supported by the combined evidence from TEM cross-sectional observations, EDS elemental mapping, UV–Vis spectroscopy, and XRD analysis, which collectively confirm the presence of Ag nanoclusters embedded within silica or zirconia matrices.

UV–Vis spectroscopy (Figure 1a), performed on model soda-lime glass substrates, confirmed the presence of silver nanoclusters embedded within both ceramic matrices. A layer of silica (SiO_2) or zirconia (ZrO_2) was used for comparison. The UV–Vis spectrum of the matrix alone coating exhibits a lack of discernible peaks. The SiO_2–Ag composite coating exhibited a well-defined surface plasmon resonance (SPR) peak at approximately 427 nm, characteristic of nanoscale silver dispersed within an amorphous oxide matrix [35]. In contrast, the ZrO_2–Ag coating showed a weaker and slightly blue-shifted SPR feature (376–385 nm), indicating differences in nanocluster [40]. XRD analysis (Figure 1b) further elucidated the structural role of the ceramic matrices.

The silica-based coatings displayed a broad amorphous halo ($2\theta = 15°–35°$), confirming the formation of an amorphous SiO_2 network. In contrast, zirconia coatings exhibited diffraction peaks at around $2\theta = 28°$, 30°, 50°, 60°, associated with the crystalline form of zirconia (PCPDF 01-074-0815) after the sputtering process. Although peak broadening in the composite coatings suggests partial amorphization induced by Ag incorporation during sputtering [41]. In both systems, characteristic Ag reflections at $2\theta \approx$ 38°, 44°, 64°, and 77° confirmed the presence of metallic silver nanoclusters (PCPDF 01-089-3722). These results demonstrate that the ceramic matrix not only embeds silver but also undergoes structural modification that directly impacts nanocluster dispersion and accessibility.

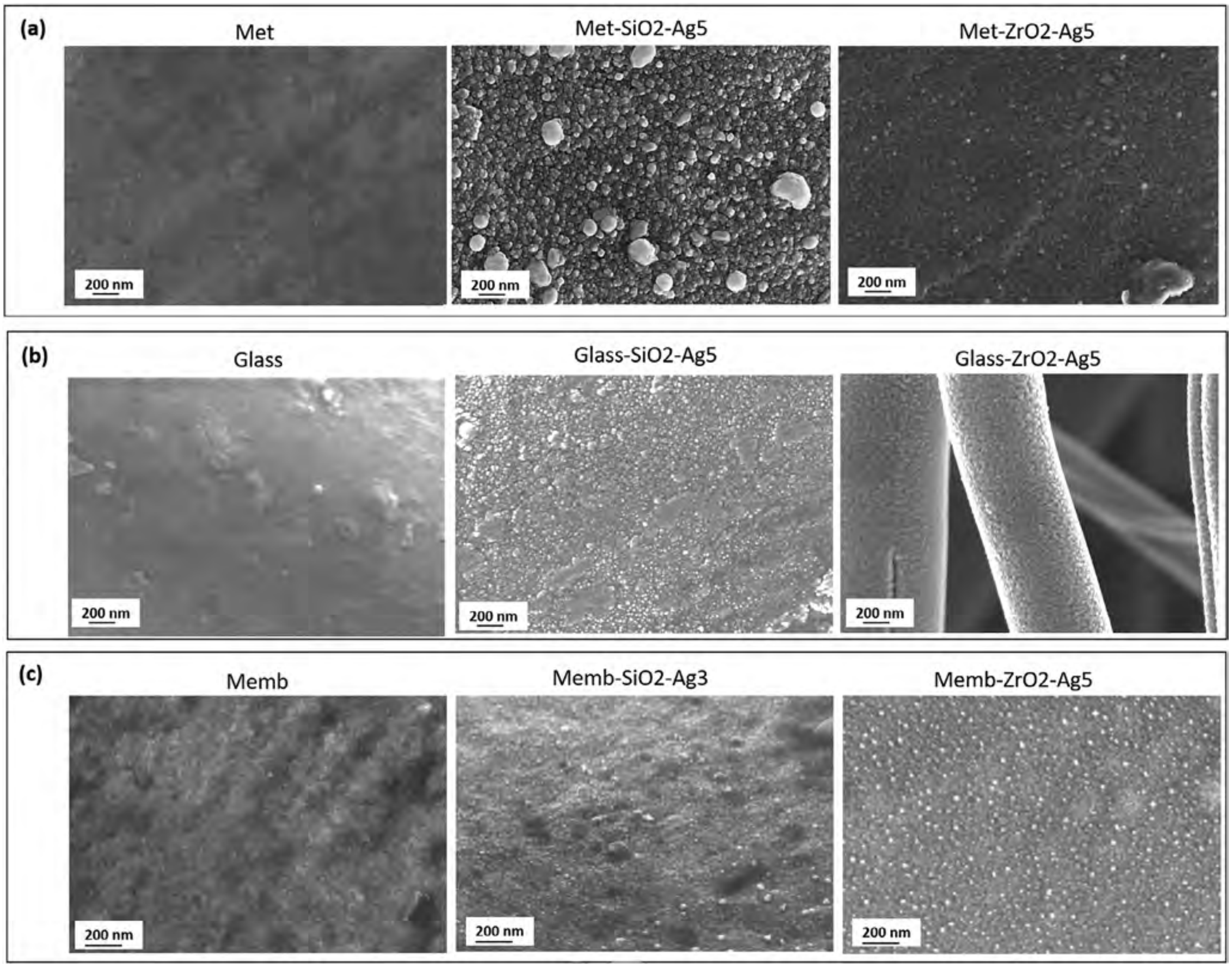

FIGURE 2 | FESEM images relative to uncoated and coated substrates with the two composite coatings of silver nanocluster/silica or zirconia matrix: (a) metallic filter Met, (b) glass-fiber filter Glass, and (c) polymeric membrane Memb.

FESEM micrographs (Figure 2) reveal pronounced matrix-dependent morphological differences, suggesting that the coating is conformal and does not visibly obstruct the filter structure at the microscale. In particular, FESEM observations of the glass-fiber substrate indicate that the coating predominantly covers the fiber surfaces rather than filling the interfiber pores, which appear largely accessible. This behavior suggests a conformal deposition without evident pore clogging at the microscale. However, it should be noted that FESEM observations alone do not provide quantitative information on pore size distribution or permeability, and therefore cannot conclusively demonstrate full preservation of filter porosity.

The images on the left show the uncoated substrates, while the images in the middle and on the right are relative to the silver nanoclusters/silica or zirconia-coated substrates, respectively.

Silica-based coatings exhibit a globular, porous morphology typical of sputtered amorphous oxides, with Ag nanoclusters appearing as bright features ranging from a few nanometers up to ~200 nm. This open ceramic structure is particularly relevant for antimicrobial applications, as it maximizes nanocluster exposure while maintaining structural integrity. Similar outcomes were obtained by Anton et al. [42] depositing silicon on Mo-based alloy through the magnetron sputtering technique. Conversely, zirconia-based coatings appear denser and more compact, with finer and more uniformly distributed Ag nanoclusters. This morphology reflects the higher packing density and structural rigidity of zirconia, which contributes to improved chemical and thermal stability.

In the polymeric membrane with silica-based coating (c), the nanoclusters are clearly visible but smaller in size, because in this case, the power applied to the silver target was lower compared to the other cases (3 W). This observation aligns with findings by Asanithi et al. [43] who demonstrated that modifying the current applied to the system used for sputtering the coating resulted in variations in the size and shape of silver nanoclusters without affecting coating performance. In the case of zirconia, it seems to be uniformly deposited across the entire sample, and the nanoclusters appear to be well-distributed within it. Overall, both coatings show a homogeneous coverage of the substrate, consistent with the conformal deposition behavior observed by FESEM.

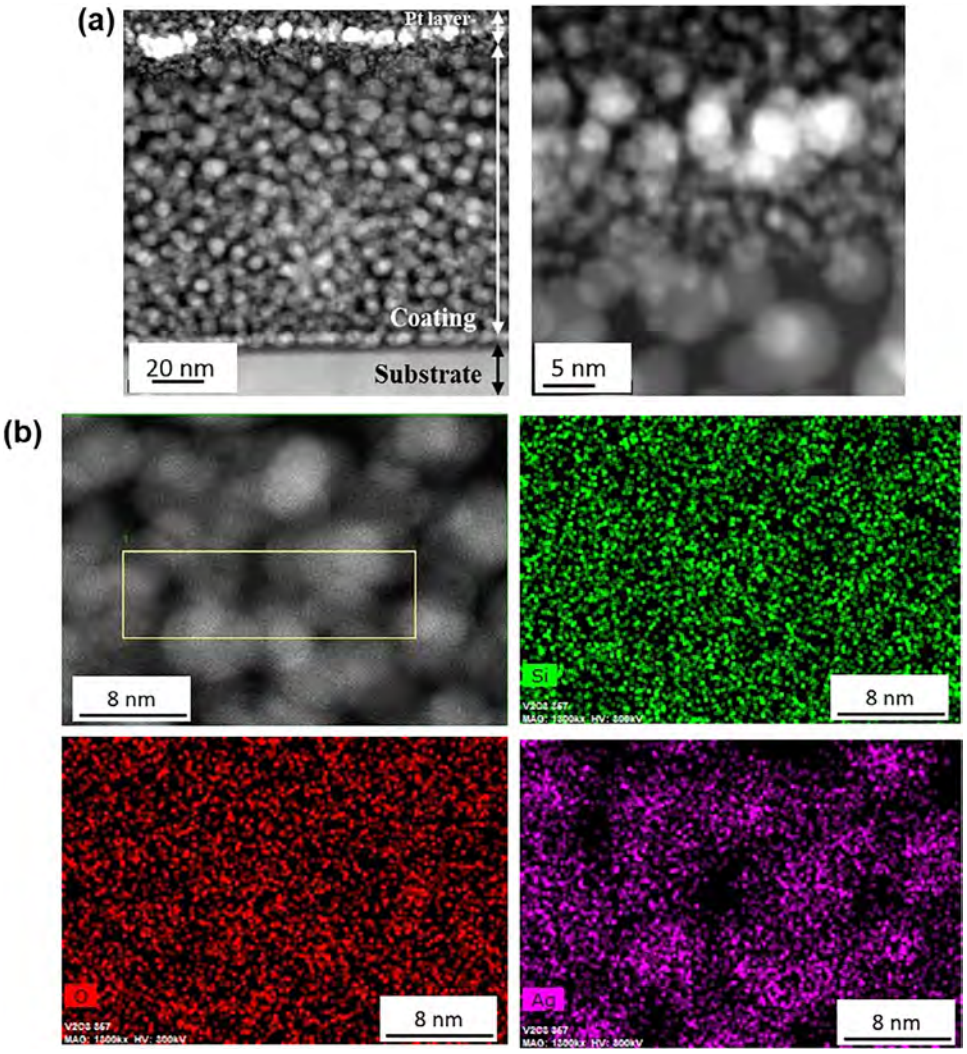

FIGURE 3 | (a) TEM analysis of silver nanocluster/silica matrix composite coating deposited on Met at different magnifications. (b) Image and relative EDS maps of Si (green), O (red), and Ag (purple).

TEM analysis (Figures 3 and 4) was conducted for a more in-depth investigation into the size, shape, and distribution of silver nanoclusters in both coatings.

In SiO_2–Ag coatings (Figure 3a), Ag nanoclusters with sizes of only a few nanometers are homogeneously dispersed within a porous amorphous silica matrix, as confirmed by EDS elemental mapping, in (Figure 3b). Green and red figures demonstrate homogenous distribution of Si and O elements, which form the silica matrix of the composite coating. In contrast, Ag represented in violet was detected in some spherical areas, corresponding to the nanoclusters embedded in the SiO_2 coating.

In ZrO_2–Ag coatings (Figure 4a), Ag nanoclusters are slightly larger (~40 nm) and more confined within the ceramic matrix, particularly near the surface region. EDS map (Figure 4b) shows a silver nanocluster, colored in yellow, embedded in the zirconia-based coating, represented by orange and green points, related to Zr and O, respectively. The images obtained by TEM in cross section allowed the measurement of the coating thickness (~100 nm for SiO_2-based and ~60 nm for ZrO_2-based coatings), further demonstrating the ability of RF co-sputtering to produce thin, conformal ceramic coatings compatible with fibrous and porous substrates.

Overall, these results demonstrate that the ceramic matrix plays a decisive role in controlling coating morphology, silver nanocluster size and dispersion, and structural stability, thereby laying the foundation for the observed differences in antimicrobial behavior and regeneration performance.

3.2 | Leaching Test

The antibacterial activity of silver–ceramic composite coatings arises from a combination of contact-mediated interactions and controlled release of Ag^+ ions. To elucidate the contribution of the ceramic matrix to ion release, leaching tests were performed in water over a 14-day period (Figure 5).

Silica-based coatings exhibited higher cumulative Ag^+ release, in a range between 0.4 and 0.6 ppm after 14 days, compared to zirconia-based coatings, whose value was about 0.2 ppm. This behavior is attributed to the amorphous and porous nature of

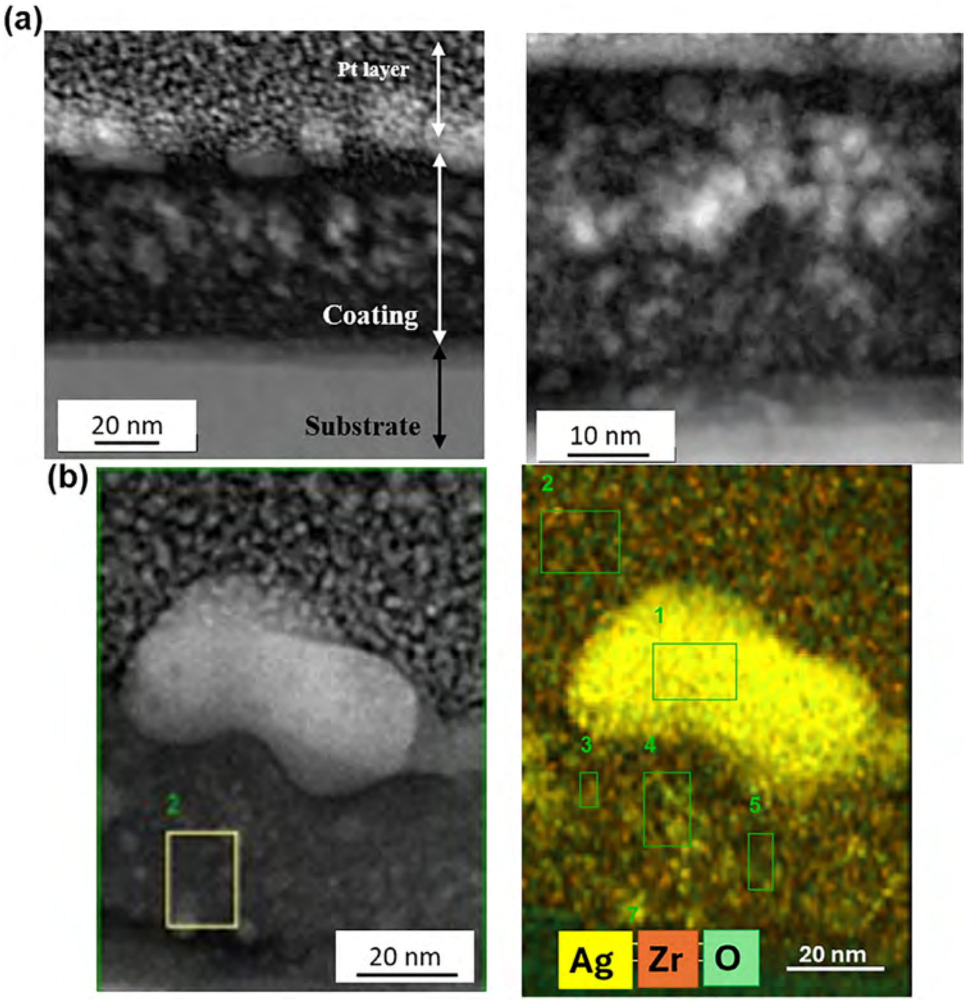

FIGURE 4 | (a) TEM analysis of silver nanocluster/zirconia matrix composite coatings deposited on Met at different magnifications. (b) Image and relative EDS map of Zr (orange), O (green), and Ag (yellow).

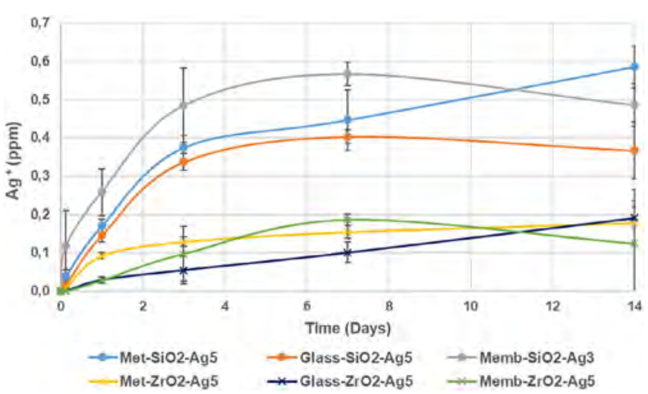

FIGURE 5 | Release test after 3 h, 1, 3, 7, and 14 days of both composite coatings deposited on metallic filter (Met-SiO2-Ag5, Met-ZrO2-Ag5), on glass-fiber filter (Glass-SiO2-Ag5, Glass-ZrO2-Ag5), and on polymeric membrane (Memb-SiO2-Ag3, Memb-ZrO2-Ag5).

the SiO_2 matrix, which facilitates water penetration and ion diffusion through its open network. In contrast, the denser ZrO_2 matrix acts as a diffusion-limiting ceramic, restricting ion mobility and resulting in a slower, more controlled release. These findings are in good agreement with previous studies reporting that coating morphology and the degree of homogeneity in Ag nanoparticle distribution play a key role in modulating ion release kinetics and, consequently, the duration and effectiveness of the antimicrobial activity [18]. Notably, polymeric membranes coated with SiO_2–Ag exhibited Ag^+ concentrations comparable to those of metallic substrates despite the lower Ag content, owing to the polymer's hydrophilicity, which enhances water uptake and ion transport. Importantly, all released Ag^+ concentrations exceed the minimum antibacterial threshold (~0.1 ppm) [44] while remaining well below cytotoxicity limits for human cells (10 ppm) [45], confirming that ceramic matrix selection enables safe and effective antimicrobial functionality. These findings demonstrate that the ceramic phase acts as a functional regulator of silver ion release, ensuring a gradual and controlled release profile.

3.3 | Antibacterial and Antifungal Tests

The antibacterial and antifungal effectiveness of silver nanoclusters/silica or zirconia composite coatings deposited on metallic, glass-fiber filters, and the polymeric membrane was qualitatively assessed by the inhibition halo test toward *S. epidermidis, E. coli, and C. albicans* (Figure 6).

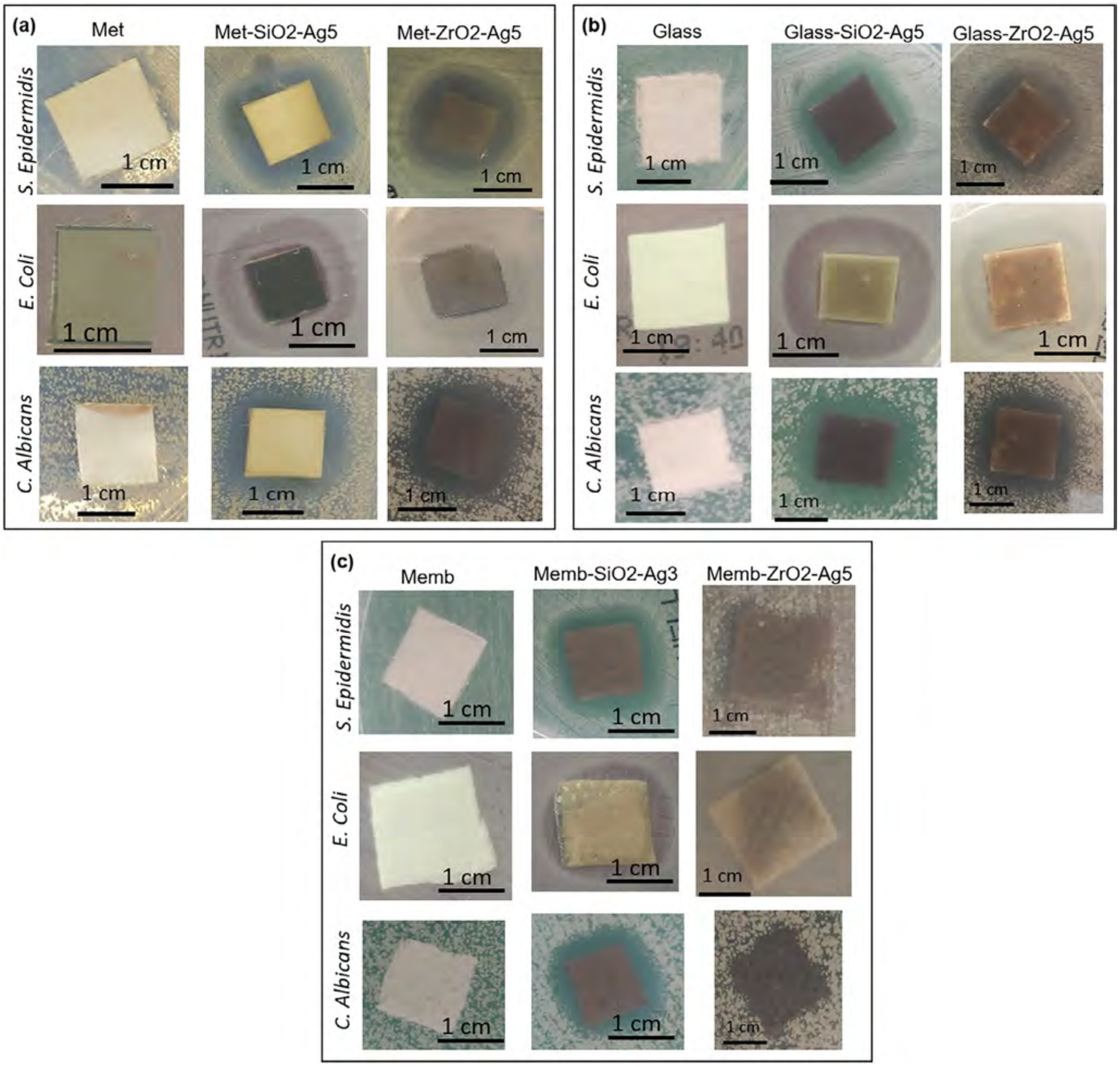

FIGURE 6 | Inhibition halo test of both silica and zirconia coatings toward *S. epidermidis*, *E. coli*, and *C. albicans* (a) on metallic filter, (b) on glass-fiber filter, and (c) on polymeric membrane.

Considering the metallic filter, both the deposited coatings are able to form an approximately 3–5 mm halo, free of bacteria, around the samples, toward all the tested microorganisms. In the presence of uncoated filters as control, the halo is not visible and microorganisms proliferated under the samples. A double halo was observed in tests against *S. epidermidis* and *E. coli*, comprising an inner area adjacent to the sample devoid of colonies, indicating complete inhibition of bacterial growth, and an outer zone where bacterial growth was slowed and partially inhibited, with some colonies visible. The phenomenon was already reported in other studies [46, 47]. Similar results were observed for the glass-fiber filter (Figure 6b). The presence of a halo (about 5 mm in size) around the coated samples confirms the bactericidal activity of the composite coatings. Regarding the polymeric membrane (Figure 6c), the antibacterial properties depend on the coating composition. In fact, a well-visible halo is present around samples coated with silver nanoclusters/silica composite coating, indicating bacterial inhibition and fungal proliferation. On the other hand, the halo is less evident with the zirconia-based coating, but bacteria are not able to proliferate in direct contact with the coated sample. As previously mentioned, uncoated samples allowed bacterial proliferation.

The second antibacterial quantitative test was performed in order to count the number of *S. epidermidis* colonies that proliferated in the presence of both coated and uncoated samples. Figure 7 shows the histograms representing the numbers of CFU proliferated in broth (a) and in solution after the vortex process (b). The red line reported in graph (a) indicates the initial number of *S. epidermidis*

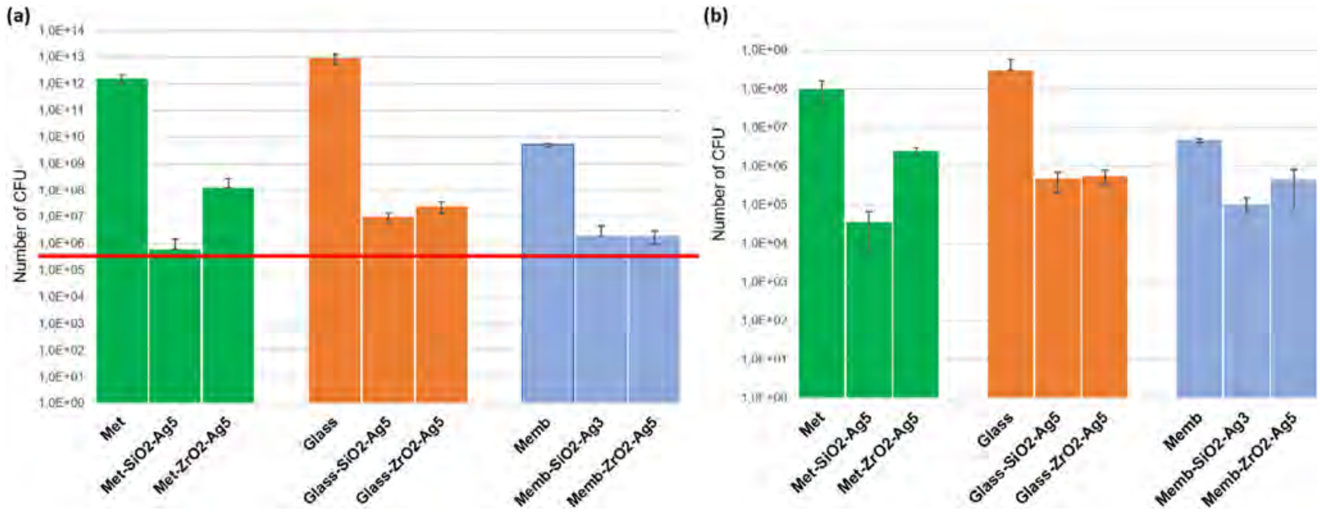

FIGURE 7 | Histograms showing the results of *S. epidermidis* CFU proliferation in broth (a) and in the vortex solution (b), for silver nanocluster/silica or zirconia composite coatings deposited on different filtration media (Met, Glass, and Memb).

TABLE 2 | CFU number counted in the bacterial broth and vortex solution.

		CFU number/mL	
Substrate	**Coating**	**Broth**	**Vortex**
Met	—	$(1.6 \pm 0.6) \times 10^{12}$	$(1.0 \pm 0.6) \times 10^{8}$
	SiO2-Ag5	$(6.2 \pm 8.5) \times 10^{5}$	$(3.6 \pm 3.0) \times 10^{4}$
	ZrO2-Ag5	$(1.3 \pm 1.5) \times 10^{8}$	$(2.5 \pm 0.6) \times 10^{6}$
Glass	—	$(9.3 \pm 3.9) \times 10^{12}$	$(2.9 \pm 3.0) \times 10^{8}$
	SiO2-Ag5	$(1.0 \pm 0.4) \times 10^{7}$	$(4.6 \pm 2.5) \times 10^{5}$
	ZrO2-Ag5	$(2.5 \pm 1.3) \times 10^{7}$	$(5.7 \pm 2.2) \times 10^{5}$
Memb	—	$(5.0 \pm 0.7) \times 10^{9}$	$(4.6 \pm 0.6) \times 10^{6}$
	SiO2-Ag3	$(1.9 \pm 2.9) \times 10^{6}$	$(1.1 \pm 0.4) \times 10^{5}$
	ZrO2-Ag5	$(1.9 \pm 1.0) \times 10^{6}$	$(4.5 \pm 3.7) \times 10^{5}$

CFU inoculated into the broth (5×10^5 CFU/mL). The related values are reported in Table 2.

Despite being applied to only one side, the coatings significantly reduced bacterial colonies across all substrates. Specifically, the presence of the silver nanoclusters/silica composite coating deposited on the metallic filter (Met-SiO2-Ag5) resulted in a substantial reduction in bacterial colony growth by 7 orders of magnitude in the broth and 4 orders of magnitude in the vortex solution, compared to the data obtained from the uncoated case. For the coating with zirconia matrix, the reduction was 4 orders of magnitude in the broth and 2 in the vortex solution. A significant reduction in bacterial proliferation up to 5 and 3 orders of magnitude for broth and vortex solutions, respectively, was also reached for glass-fiber filters, demonstrating strong antibacterial activity unaffected by the coating matrix. Regarding the polymeric membrane, no remarkable differences were observed between the two solutions for both coatings, even with the lower amount of silver in Memb-SiO2-Ag3. Similarly, the matrix did not significantly affect the overall antibacterial performance under the tested conditions, consistent with previous findings. Nevertheless, the choice of the ceramic matrix significantly influenced coating morphology, silver ion release kinetics, and performance under severe contamination conditions, highlighting distinct functional roles for silica and zirconia.

The third and most rigorous antibacterial test simulated severe contamination conditions. Filters were exposed to a highly concentrated *S. epidermidis* solution (McFarland index 5.0), delivered using a bioaerosol generator. Although the contamination was initially conducted at different times (5, 10, and 30 min), the results presented here are specific to the most stringent conditions of 30 min. Figure 8 shows the consistent outcomes obtained across all the studied material types and confirms the strong antibacterial effect of the analyzed coatings.

Under these rigorous conditions, the silica-based coatings successfully and completely inhibited the proliferation of bacteria on all types of substrates, contrasting with the visible bacterial growth observed around and in contact with the uncoated samples. The coating composed of a zirconia matrix reduced the contamination without completely inhibiting the proliferation, as some colonies appear close to the sample.

Quantitative analysis of colonies proliferated in the presence of uncoated and coated samples, for broth and vortex solutions, shown in Figure 8b, confirms the strong bactericidal effectiveness of both silica-based and zirconia-based coatings. Table 3 summarizes the values obtained.

In the case of uncoated filters, bacterial proliferation reached 10^{11}–10^{12} CFU/mL in the broth-immersed sample, which was significantly reduced by the coatings. For the Met-ZrO2-Ag5, no colonies were counted in the broths, probably because the order of magnitude to be considered was 10^2, as confirmed by the counts after the vortex process. In the case of the Glass-SiO2-Ag5 sample, CFU were reduced of 11 orders of magnitude, while a higher number of CFUs (10^4 orders of magnitude) was detected in the presence of the zirconia-based coating (Glass-ZrO2-Ag5). For Memb samples, the number of proliferated colonies in the broths

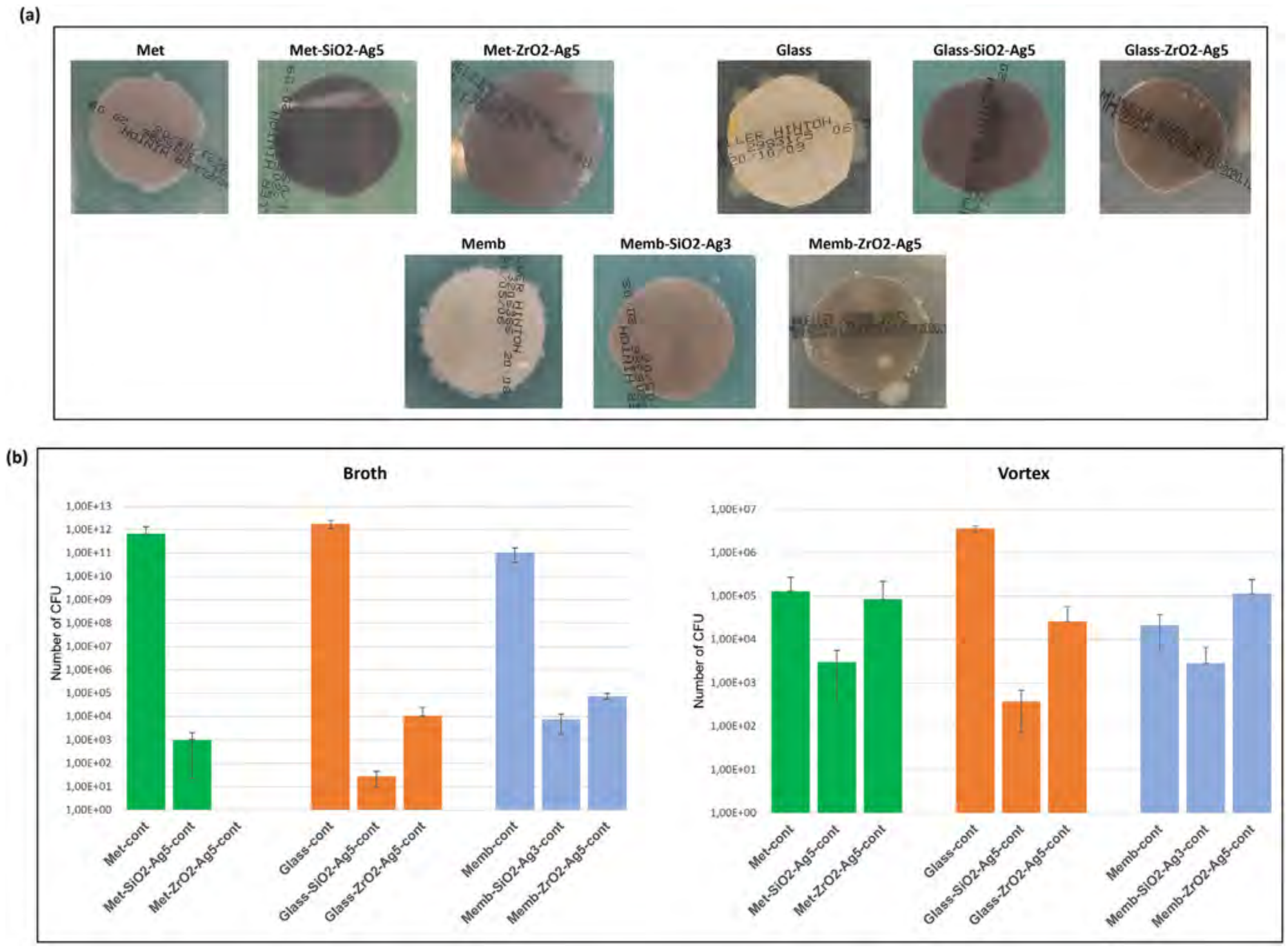

FIGURE 8 | (a) Photographs relative to both coated and uncoated filters after contamination of 30 min with *S. epidermidis* bioaerosol generator on metallic filter, glass-fiber filter, and polymeric membrane. (b) Histograms relative to the results of CFU proliferated in broth and into the vortex solution for silica/silver coating and zirconia/silver coating after 30 min contamination.

TABLE 3 | CFU number counted in the bacterial broth and vortex solution with contaminated samples.

		CFU number/mL	
Substrate	**Coating**	**Broth**	**Vortex**
Met	—	$(6.6 \pm 0.7) \times 10^{11}$	$(1.3 \pm 1.4) \times 10^{5}$
	SiO2-Ag5	$(1.0 \pm 1.0) \times 10^{3}$	$(3.7 \pm 2.6) \times 10^{3}$
	ZrO2-Ag5	0.0×10^{3}	$(8.4 \pm 0.1) \times 10^{5}$
Glass	—	$(1.8 \pm 0.7) \times 10^{12}$	$(3.6 \pm 0.5) \times 10^{6}$
	SiO2-Ag5	$(2.8 \pm 1.8) \times 10^{1}$	$(3.7 \pm 3.0) \times 10^{2}$
	ZrO2-Ag5	$(1.1 \pm 1.3) \times 10^{4}$	$(2.6 \pm 3.1) \times 10^{4}$
Memb	—	$(1.0 \pm 0.6) \times 10^{11}$	$(2.1 \pm 1.6) \times 10^{4}$
	SiO2-Ag3	$(7.3 \pm 5.5) \times 10^{3}$	$(2.8 \pm 3.6) \times 10^{3}$
	ZrO2-Ag5	$(7.5 \pm 1.9) \times 10^{4}$	$(1.1 \pm 1.2) \times 10^{5}$

is significantly lower in the presence of the coatings compared to the as-received filter. In the case of vortex solutions, a higher number of colonies adhered to the ZrO_2/Ag coating was observed compared to the uncoated filter.

The enhanced antibacterial activity of ceramic coatings with antimicrobial agents is widely studied in literature [48–51], and in particular, the antibacterial activity of silver nanoclusters against both Gram-positive and Gram-negative bacteria is well established. Although the precise mechanism is not fully understood, it is generally attributed to the ability of silver nanoparticles and Ag^{+} ions to interact with bacterial cell walls, penetrate the cells, and generate reactive oxygen species (ROS), ultimately inducing cell apoptosis [52–55]. These results highlight that the incorporation of Ag into glass–ceramic composites enhances the antimicrobial properties of the coatings, consistent with previous studies [18]. Recently, Acharya et al. [56] compared the bactericidal activity of silver nanoparticles and Ag-SiO_2 core–shell systems against *Bacillus subtilis*, *S. aureus*, *Serratia marcescens*, and *Klebsiella pneumoniae*, finding that both NPs exhibited an antibacterial effect, but it was enhanced with Ag@SiO2 system, due to a prolonged release of ions through the porous silica shell, and to silver nanoparticles attached on the surface. A hybrid material composed of silica nanospheres decorated with silver nanoparticles (AgNP@SiO2), atomized onto air filters and exposed to bacterial aerosols, demonstrated the ability to trap both *S. epidermidis* and *E.coli* bacteria, destroying their cell walls in an attempt to free themselves. In addition, bare silver nanoparticles can create a groove on the membrane of

Gram-negative bacteria, while AgNP@SiO2 acts upon contact with the cell wall [57]. In this work, silver nanoclusters are not only exposed on the surface, but they are well distributed within a porous silica matrix. For this reason, the antibacterial effect is likely due to the action of nanoclusters themselves and ions released from the coating in a controlled and gradual manner, allowing for prolonged bactericidal effects over time.

The inhibition of Ag-SiO_2 nanoparticles of *C. albicans* was tested by Rossi et al. [58], who found that the minimum inhibition concentration in the presence was 1000 µg/mL.

Zirconia-based systems, while typically exhibiting a slower ion-release kinetics due to their denser and more crystalline structure, have also demonstrated strong antibacterial and antifungal activity when combined with silver. ZrO_2 nanoparticles functionalized with dihydroquercetin (DHQ) and decorated with Ag nanoparticles showed significant antibacterial effects against *S. aureus* and *E. coli*, with activity dependent on exposure time and concentration [59]. Core–shell silver–zirconia nanoparticles were reported to exhibit strong bactericidal activity against *E. coli* and *S. aureus*, as well as antifungal activity against *C. albicans* [60]. Furthermore, ceramic Ag-deposited ZrO_2 coatings applied on stainless steel substrates demonstrated pronounced antibacterial efficacy against *S. aureus* and *E. coli*, together with excellent corrosion resistance [61], a property that is crucial for durable and reusable applications.

In this context, recent studies on Ag-deposited ZrO_2 coatings on 316L stainless steel provide additional insight into the multifunctional advantages of zirconia-based ceramic coatings. These works highlighted that Ag-deposited ZrO_2 surfaces exhibit a pronounced hydrophobic character compared to both bare 316L and ZrO_2-only coatings, indicating that surface engineering can effectively tailor wettability, with important implications for antibacterial performance and fouling resistance. High adhesion strength values (first failure at ~170 N) and improved corrosion resistance were also reported, with the coated systems behaving similarly to passive materials after repeated corrosion cycles. In addition to enhanced corrosion protection, these coatings showed clear antibacterial activity against *S. aureus* and *E. coli*, confirming that surface-modified ZrO_2/Ag systems can effectively inhibit bacterial adhesion and growth, thereby reducing the risk of biofilm formation.

From an application perspective, particularly for air filtration systems, the antibacterial mechanism is strongly influenced by the operating environment. In low-humidity conditions typical of HVAC systems and respirators, the dominant antimicrobial pathway is generally attributed to contact-killing at the air–solid interface, while Ag^+ ion release plays a complementary role. This distinction is critical, as aqueous-phase diffusion is limited under aerosol exposure. Studies on silver–copper nanolayers exposed to bacterial and viral aerosols reported > 90% pathogen reduction within hours, primarily due to direct surface contact rather than ion leaching [62]. Similarly, sputtered silver nanocluster/silica coatings applied to FFP3 masks demonstrated rapid virucidal activity against SARS-CoV-2, with the antimicrobial effect explicitly linked to contact-based mechanisms [32].

3.4 | Thermal Treatment for Filter Regeneration

A subsequent contamination test was conducted on both metallic and glass-fiber-based filters after subjecting them to a thermal regeneration treatment at 200°C, aimed at evaluating whether the antibacterial activity of the coatings remained effective following a high-temperature sterilization process. The polymeric membrane was excluded from the regeneration study due to its limited thermal stability at 200°C, which would compromise its structural integrity. Therefore, the proposed regeneration strategy is currently applicable only to thermally stable substrates such as metallic and glass-fiber filters. The extension of this approach to polymer-based filters would require alternative, lower-temperature or nonthermal regeneration methods, which will be explored in future work.

This regeneration method was selected in place of conventional sterilization processes, such as autoclaving at 121°C, because these involve high humidity and pressure conditions that could adversely affect the stability and adhesion of the nanostructured coatings. In contrast, the applied dry heat protocol allows effective decontamination without introducing moisture or mechanical stress, making it more suitable for preserving the performance of ceramic-based composite coatings. The results of this test provide compelling evidence that the coatings developed in this study can withstand a regeneration process after bioaerosol contamination. Consequently, the filters can be reused multiple times without significant deterioration in their antibacterial performance. Figure 9 reports the results of the contamination test conducted on filters that were initially contaminated, then subjected to thermal regeneration, and subsequently contaminated again for 30 min.

The remarkable inhibition or reduction of bacterial growth achieved by the presence of silver nanoclusters within both coatings is evident. This contrasts starkly with the higher levels of bacterial proliferation observed around the uncoated filters. Importantly, it is noteworthy that no significant differences can be discerned between the two matrices in both cases: following the initial contamination and after the contamination after the thermal treatment. This consistency further underscores the robustness and stability of the antibacterial performance of the coatings.

Quantitative results, shown in Figure 9b and Table 4, further confirm these observations. The related numerical values are indicated in Table 4. The heat treatment did not affect the efficacy of the coatings in inhibiting bacterial proliferation. Both coatings demonstrated that after thermal sterilization processes, they maintained their antibacterial behavior, and no substantial differences were detected between the two matrices under examination. The reduction of colonies proliferated in the broths was approximately 8 or 9 orders of magnitude compared to the uncoated filters, while after the vortex process, the number of counted colonies in the presence of the coatings is reduced by approximately 1–2 orders of magnitude. The results obtained, in this case as well, confirm that the choice between the two matrices does not have a decisive influence on the effect obtained.

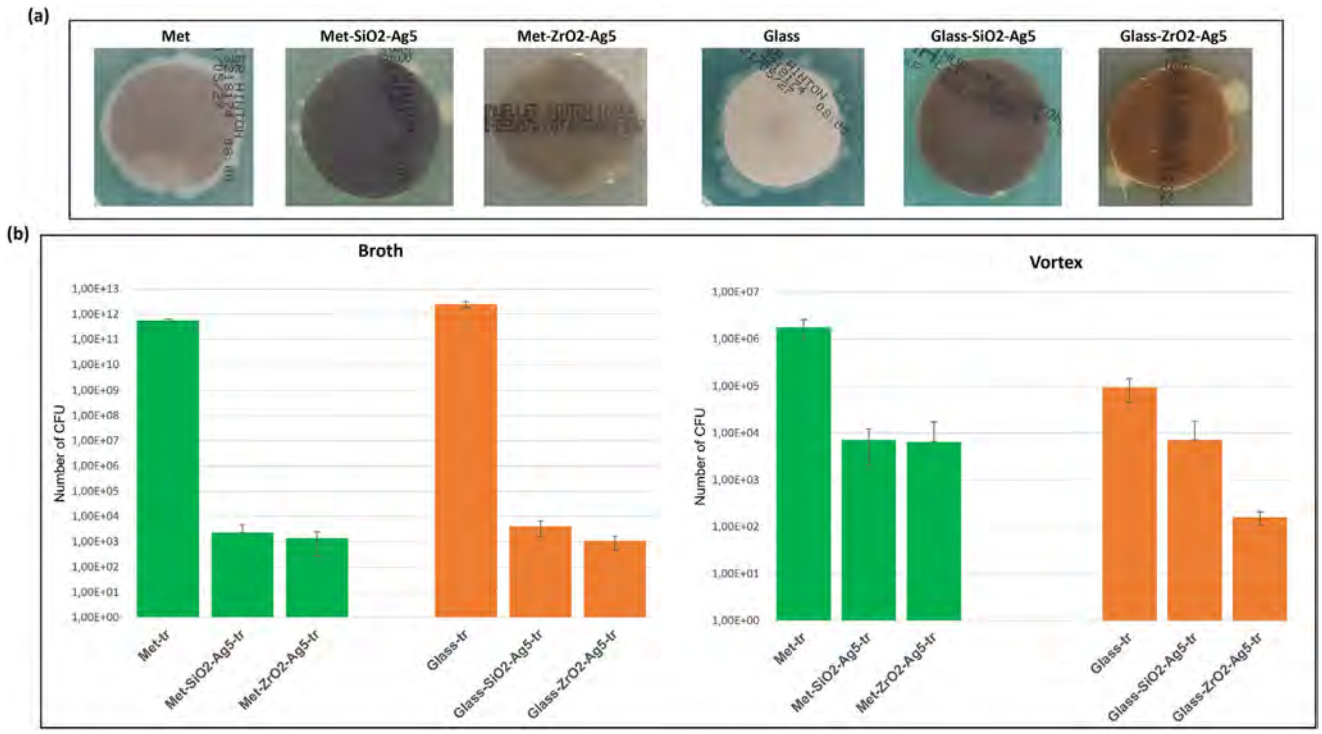

FIGURE 9 | Photographs relative to both coated and uncoated filters for 30 min with bioaerosol generator after thermal regeneration and second bacterial contamination on both silica and zirconia composite coatings, on metallic and glass-fiber filters. (b) Histograms relative to the results of CFU proliferated in broth and into the vortex solution for silica/silver coating and zirconia/silver coating after thermal regeneration and second bacterial contamination.

TABLE 4 | CFU number counted in the bacterial broth and vortex solution with thermal regenerated samples.

Substrate	Coating	CFU number/mL	
		Broth	Vortex
Met	—	$(5.6 \pm 0.7) \times 10^{11}$	$(1.8 \pm 0.8) \times 10^{6}$
	SiO2-Ag5	$(2.3 \pm 2.5) \times 10^{3}$	$(7.3 \pm 5.1) \times 10^{3}$
	ZrO2-Ag5	$(1.4 \pm 1.1) \times 10^{3}$	$(6.5 \pm 0.1) \times 10^{3}$
Glass	—	$(2.5 \pm 0.7) \times 10^{12}$	$(9.5 \pm 5.0) \times 10^{4}$
	SiO2-Ag5	$(4.1 \pm 2.6) \times 10^{3}$	$(7.2 \pm 0.1) \times 10^{3}$
	ZrO2-Ag5	$(1.1 \pm 0.6) \times 10^{3}$	$(1.6 \pm 4.9) \times 10^{2}$

This work evaluates a sterilization technique for air filters that is an alternative to the more common and economical methods, which involve the use of water or water and ethanol solutions [22, 63]. The choice of a thermal treatment of three cycles at 200°C was made considering standard sterilization processes were typically conducted at 121°C in an autoclave, where there is also an effect due to the pressure. In this case, a dry method involving higher temperatures for multiple cycles was used to avoid prolonged contact with water or aqueous solutions. The effectiveness against *S. epidermidis* was then evaluated, while the effect of thermal treatment on *E. coli* was previously assessed by Kim et al. [64]. They developed a virucidal and bactericidal air filter that could be thermally sterilized by exploiting the Joule effect of a heating layer that can be heated up to 100°C. A similar system was used for facial masks to avoid the use of chemical products for the disinfection and inactivation of *E. coli* [65].

4 | Conclusions

In this study, antibacterial ceramic-based composite coatings composed of silver nanoclusters embedded in silica or zirconia oxide matrices were successfully developed and deposited via co-sputtering onto three different filtration substrates: metallic filters, glass-fiber filters, and polymeric membranes. The coatings exhibited uniform morphology and composition, as confirmed by cross-sectional FESEM and TEM analyses, while preserving the porous structure of the underlying filters.

The presence of silver nanoclusters was validated through UV–Vis and XRD analyses, and their gradual release in aqueous environments ensured a sustained antimicrobial effect over time, without exceeding cytotoxicity thresholds. Antimicrobial efficacy was rigorously demonstrated against Gram-positive (*S. epidermidis*), Gram-negative (*E. coli*) bacteria, and the fungal strain *C. albicans* using inhibition halo assays, CFU quantification, and aerosol contamination simulations.

A key innovation of this work lies in the dual comparative assessment of silica- and zirconia-based matrices across multiple substrates, under both standard and thermally regenerated conditions. Notably, the coatings maintained excellent antibacterial activity even after high-temperature regeneration cycles at 200°C, highlighting their thermal resilience and supporting their reuse potential. Although the coatings are characterized by nanoscale thickness (60–100 nm) and conformal morphology, suggesting minimal impact on airflow resistance, a quantitative assessment of pressure drop and air permeability was not performed in this study. These parameters are critical for practical applications and will be systematically investigated in future work.

Among the two matrices, ZrO_2-based coatings demonstrated lower silver ion release and greater structural stability, making them particularly suitable for humid environments or repeated sterilization cycles.

Importantly, the ceramic nature of the system is confined to the nanocomposite coating, enabling ceramic-like thermal stability while preserving the flexibility and functionality of conventional air filter substrates. These findings offer a significant advancement in the design of durable, regenerable, and multifunctional antimicrobial coatings for air filtration. The proposed approach, combining material versatility, thermal resistance, and long-term antimicrobial efficacy, opens up promising applications in HVAC systems, industrial and medical air purification units, and wearable filtration technologies such as reusable face masks and respiratory devices.

Future work will focus on comprehensive functional validation under real operating conditions, including pressure drop analysis, dust-loading performance, and mechanical endurance across multiple regeneration cycles. Environmental impact assessments related to long-term silver release will also be prioritized to ensure sustainable deployment.

Acknowledgments

This work was partially funded by FinPiemonte within the project entitled "BIO-kILLER—Anti-BIOpollutant coatIng for reusable fiLtER" (Manunet III Transnational Call (2018), MNET18/OTHR3507) and by the program KMM-VIN RESEARCH FELLOWSHIPS 2023 that contributes to enhance existing networks of beneficial research collaborations between the authors. A special thanks to GV Filtri srl for supporting the research.

Open access publishing facilitated by Politecnico di Torino, as part of the Wiley - CRUI-CARE agreement.

Data Availability Statement

Data sharing not applicable to this article as no datasets were generated or analyzed during the current study.

References

1. K. Clarke, H.-O. Kwon, and S.-D. Choi, "Fast and Reliable Source Identification of Criteria Air Pollutants in an Industrial city," *Atmospheric Environment* 95 (2014): 239–248, https://doi.org/10.1016/j.atmosenv.2014.06.040.

2. N. Kalogerakis, D. Paschali, V. Lekaditis, A. Pantidou, K. Eleftheriadis, and M. Lazaridis, "Indoor Air Quality—Bioaerosol Measurements in Domestic and Office Premises," *Journal of Aerosol Science* 36, no. 5–6 (2005): 751–761, https://doi.org/10.1016/j.jaerosci.2005.02.004.

3. J. Douwes, P. Thorne, N. Pearce, and D. Heederik, "Bioaerosol Health Effects and Exposure Assessment: Progress and Prospects," *Annals of Occupational Hygiene* 47, no. 3 (2003): 187–200, https://doi.org/10.1093/annhyg/meg032.

4. T. Reponen, S. A. Grinshpun, K. L. Conwell, J. Wiest, and M. Anderson, "Aerodynamic Versus Physical Size of Spores: Measurement and Implication for Respiratory Deposition," *Grana* 40, no. 3 (2001): 119–125, https://doi.org/10.1080/00173130152625851.

5. J. P. G. Van Leuken, A. N. Swart, A. H. Havelaar, A. Van Pul, W. Van der Hoek, and D. Heederik, "Atmospheric Dispersion Modelling of Bioaerosols That Are Pathogenic to Humans and Livestock—A Review to Inform Risk Assessment Studies," *Microbial Risk Analysis* 1 (2016): 19–39, https://doi.org/10.1016/j.mran.2015.07.002.

6. Siddharth and R. Siddhartha, "Advanced Applications and Processing Techniques for Porous Ceramics," in *Advanced Smart and Multifunctional Materials Volume 2: Advanced Processing, Polymers, Ceramics, and Related Functional Materials* (American Chemical Society, 2025), pp. 1–41, https://doi.org/10.1021/bk-2025-1514.ch001.

7. N. Labhsetwar, P. Doggali, S. Rayalu, R. Yadav, T. Mistuhashi, and H. Haneda, "Ceramics in Environmental Catalysis: Applications and Possibilities," *Chinese Journal of Catalysis* 33, no. 9 (2012): 1611–1621, https://doi.org/10.1016/S1872-2067(11)60440-3.

8. M. Ross, A. Hoff, W. M. Hochstedler, et al., "Ceramic High Efficiency Particulate Air (HEPA) Filter Research and Development at Lawrence Livermore National Laboratory," *ACS Chemical Health & Safety* 32, no. 4 (2025): 383–401, https://doi.org/10.1021/acs.chas.4c00131.

9. A. Iqbal and G. Moskal, "Recent Development in Advance Ceramic Materials and Understanding the Mechanisms of Thermal Barrier Coatings Degradation," *Archives of Computational Methods Engineering* 30, no. 8 (2023): 4855–4896, https://doi.org/10.1007/s11831-023-09960-7.

10. Y. Ciawi and K. Khoiruddin, "Low-Cost Antibacterial Ceramic Water Filters for Decentralized Water Treatment: Advances and Practical Applications," *ACS Omega* 9, no. 11 (2024): 12457–12477, https://doi.org/10.1021/acsomega.3c09311.

11. S. P. Rivera-Sánchez, I. D. Ocampo-Ibáñez, J. A. Silva-Leal, et al., "A Novel Filtration System Based on Ceramic Silver-Impregnated Pot Filter Combined With Adsorption Processes to Remove Waterborne Bacteria," *Scientific Reports* 10 (2020): 11198, https://doi.org/10.1038/s41598-020-68192-y.

12. L. Mpenyana-Monyatsi, N. H. Mthombeni, M. S. Onyango, and M. N. B. Momba, "Cost-Effective Filter Materials Coated With Silver Nanoparticles for the Removal of Pathogenic Bacteria in Groundwater," *International Journal of Environmental Research and Public Health* 9, no. 1 (2012): 244–271, https://doi.org/10.3390/ijerph9010244.

13. J. Ren, R. Gao, A. Li, et al., "Efficient Air Purification Using Porous Ceramic-Based Bubble-Enhanced Filtration System," *Communications Engineering* 5 (2025): 4, https://doi.org/10.1038/s44172-025-00559-3.

14. B. Pietrzyk and S. Miszczak, "Functional Ceramic Coatings," *Coatings* 11, no. 2 (2021): 130, https://doi.org/10.3390/coatings11020130.

15. H. R. A. R. Abadi, M. K. Aminian, and S. K. Fatah, "Multifunctional Silica-Based Coatings for Ceramic Tiles: Balancing Hydrophobicity and Aesthetics," *International Journal of Applied Ceramic Technology* 22, no. 6 (2025): e70037, https://doi.org/10.1111/ijac.70037.

16. K. Taechasirivichai, S. Chiarakorn, C. Chawengkijwanich, T. Pongprayoon, and S. Chuangchote, "Ceramic Tiles Coated With Zr-Ag Co-Doped TiO_2 Thin Film for Indoor Air Purifying and Antimicrobial Applications," *International Journal of Applied Ceramic Technology* 20, no. 3 (2023): 2019–2029, https://doi.org/10.1111/ijac.14295.

17. A. S. Rodrigues, J. G. S. Batista, M. Á. V. Rodriguesì, et al., "Advances in Silver Nanoparticles: A Comprehensive Review on Their Potential as Antimicrobial Agents and Their Mechanisms of Action Elucidated by Proteomics," *Frontiers in Microbiology* 15 (2024), 1440065, https://doi.org/10.3389/fmicb.2024.1440065.

18. S. Singh, A. Gurjar, E. Bhatia, et al., "Tailoring Antimicrobial Characteristic and Mechanical Behavior With Silver in Leucite–Glass–Ceramics for Hard Tissue Engineering," *International Journal of Applied Ceramic Technology* 21, no. 3 (2024): 2081–2093, https://doi.org/10.1111/ijac.14617.

19. W. Wang, R. Guo, C. Niu, Z. Zhao, and K. Xu, "Diffusion and Release Behavior of ag in Ion-Exchanged Antibacterial Glaze," *International Journal of Applied Ceramic Technology* 21 (2024): 2094–2101, https://doi.org/10.1111/ijac.14663.

20. N. M. Possolli, H. Borba Modolon, H. Mendes de Souza, et al., "Antimicrobial Characteristics of the Li_2O–ZrO_2–Si_2O Bioactive Glass and Glass-Ceramic for Bone Regeneration and Wound Healing," *International Journal of Applied Ceramic Technology* 21, no. 3 (2024): 2567–2577, https://doi.org/10.1111/ijac.14709.

21. D. Y. Choi, K. J. Heo, J. Kang, et al., "Washable Antimicrobial Polyester/Aluminum Air Filter With a High Capture Efficiency and Low Pressure Drop," *Journal of Hazardous Materials* 351 (2018): 29–37, https://doi.org/10.1016/j.jhazmat.2018.02.043.

22. Y. H. Choi, M.-J. Kim, J. Lee, J.-C. Pyun, and D.-Y. Khang, "Recyclable, Antibacterial, Isoporous Through-Hole Membrane Air Filters With Hydrothermally Grown ZnO Nanorods," *Nanomaterials* 11, no. 12 (2021): 3381, https://doi.org/10.3390/nano11123381.

23. V. Sujitha, K. Murugan, M. Paulpandi, et al., "Green-Synthesized Silver Nanoparticles as a Novel Control Tool Against Dengue Virus (DEN-2) and Its Primary Vector Aedes aegypti," *Parasitology Research* 114, no. 9 (2015): 3315–3325, https://doi.org/10.1007/s00436-015-4556-2.

24. N. H. Shady, A. R. Khattab, S. Ahmed, et al., "Hepatitis C Virus NS3 Protease and Helicase Inhibitors From Red Sea Sponge (*Amphimedon*) Species in Green Synthesized Silver Nanoparticles Assisted by in Silico Modeling and Metabolic Profiling," *International Journal Nanomedicine* 15 (2020): 3377–3389, https://doi.org/10.2147/IJN.S233766.

25. S. S. Salem and A. Fouda, "Green Synthesis of Metallic Nanoparticles and Their Prospective Biotechnological Applications: An Overview," *Biological Trace Element Research* 199, no. 1 (2021): 344–370, https://doi.org/10.1007/s12011-020-02138-3.

26. Y. Mehmood, U. Farooq, H. Yousaf, et al., "Antiviral Activity of Green Silver Nanoparticles Produced Using Aqueous Buds Extract of *Syzygium aromaticum*," *Supplement, Pakistan Journal of Pharmaceutical Sciences* 33, no. S2 (2020): 839–845, https://doi.org/10.36721/PJPS.2020.33.2.SUP.839-845.1.

27. H. R. Byun, S. Y. Park, E. T. Hwang, et al., "Antimicrobial Air Filter Coating With Plant Extracts against Airborne Microbes," *Applied Sciences* 10, no. 24 (2020): 9120, https://doi.org/10.3390/app10249120.

28. M. Akhtar, S. A. Uzair, M. Rizwan, and M. A. Ur Rehman, "The Improvement in Surface Properties of Metallic Implant via Magnetron Sputtering: Recent Progress and Remaining Challenges," *Frontiers in Materials* 8 (2022), 747169, https://doi.org/10.3389/fmats.2021.747169.

29. X.-Q. Tan, J.-Y. Liu, J.-R. Niu, J.-Y. Liu, and J.-Y. Tian, "Recent Progress in Magnetron Sputtering Technology Used on Fabrics," *Materials* 11, no. 10 (2018): 1953, https://doi.org/10.3390/ma11101953.

30. C. Balagna, S. Perero, F. Bosco, C. Mollea, M. Irfan, and M. Ferraris, "Antipathogen Nanostructured Coating for Air Filters," *Applied Surface Science* 508 (2020): 145283, https://doi.org/10.1016/j.apsusc.2020.145283.

31. C. Balagna, R. Francese, S. Perero, D. Lembo, and M. Ferraris, "Nanostructured Composite Coating Endowed With Antiviral Activity Against Human Respiratory Viruses Deposited on Fibre-Based Air Filters," *Surface & Coatings Technology* 409 (2021): 126873, https://doi.org/10.1016/j.surfcoat.2021.126873.

32. C. Balagna, S. Perero, E. Percivalle, E. V. Nepita, and M. Ferraris, "Virucidal Effect Against Coronavirus SARS-CoV-2 of a Silver Nanocluster/Silica Composite Sputtered Coating," *Open Ceramics* 1 (2020): 100006, https://doi.org/10.1016/j.oceram.2020.100006.

33. C. Balagna, M. Irfan, S. Perero, et al., "Characterization of Antibacterial Silver Nanocluster/Silica Composite Coating on High Performance Kevlar® Textile," *Surface & Coatings Technology* 321 (2017): 438–447, https://doi.org/10.1016/j.surfcoat.2017.05.009.

34. A. Luceri, S. Perero, A. Cochis, et al., "Washing Resistant Antibacterial Composite Coatings on Cotton Textiles," *Cellulose* 30, no. 15 (2023): 9877–9897, https://doi.org/10.1007/s10570-023-05471-7.

35. M. Irfan, S. Perero, M. Miola, et al., "Antimicrobial Functionalization of Cotton Fabric With Silver Nanoclusters/Silica Composite Coating via RF Co-Sputtering Technique," *Cellulose* 24, no. 5 (2017): 2331–2345, https://doi.org/10.1007/s10570-017-1232-y.

36. G. Pradhaban, G. S. Kaliaraj, and V. Vishwakarma, "Antibacterial Effects of Silver–Zirconia Composite Coatings Using Pulsed Laser Deposition Onto 316L SS for Bio Implants," *Progress in Biomaterials* 3, no. 2–4 (2014): 123–130, https://doi.org/10.1007/s40204-014-0028-5.

37. M. Ferraris, C. Balagna, and S. Perero, "Method for the Application of an Antiviral Coating to a Substrate and Relative Coating," WO2019082001 (2019).

38. NCCLS M2-A9, *Performance Standards for Antimicrobial Disk Susceptibility Tests, Approved Standard*, 9th ed. (NCCLS, 2003).

39. NCCLS M7-A6, *Methods for Dilution Antimicrobial Susceptibility Tests for Bacteria That Grow Aerobically, Approved Standard*, 6th ed. (NCCLS, 2003).

40. M. Kumar and G. B. Reddy, "Tailoring Surface Plasmon Resonance in Ag:ZrO_2 Nanocomposite Thin Films," *Physica E: Low-Dimensional Systems and Nanostructures* 43, no. 1 (2010): 470–474, https://doi.org/10.1016/j.physe.2010.08.031.

41. C. Balagna, S. Perero, S. Ferraris, et al., "Antibacterial Coating on Polymer for Space Application," *Materials Chemistry and Physics* 135, no. 2–3 (2012): 714–722, https://doi.org/10.1016/j.matchemphys.2012.05.049.

42. R. Anton, N. Laska, U. Schulz, S. Obert, and M. Heilmaier, "Magnetron Sputtered Silicon Coatings as Oxidation Protection for Mo-Based Alloys," *Advanced Engineering Materials* 22, no. 7 (2020): 2000218, https://doi.org/10.1002/adem.202000218.

43. P. Asanithi, S. Chaiyakun, and P. Limsuwan, "Growth of Silver Nanoparticles by DC Magnetron Sputtering," *Journal Nanomaterials* 2012 (2012): e963609, https://doi.org/10.1155/2012/963609.

44. W. Chen, Y. Liu, H. S. Courtney, et al., "In Vitro Anti-Bacterial and Biological Properties of Magnetron Co-Sputtered Silver-Containing Hydroxyapatite Coating," *Biomaterials* 27, no. 32 (2006): 5512–5517, https://doi.org/10.1016/j.biomaterials.2006.07.00.

45. K. Jamuna-Thevi, S. A. Bakar, S. Ibrahim, N. Shahab, and M. R. M. Toff, "Quantification of Silver Ion Release, In Vitro Cytotoxicity and Antibacterial Properties of Nanostuctured Ag Doped TiO_2 Coatings on Stainless Steel Deposited by RF Magnetron Sputtering," *Vacuum* 86, no. 3 (2011): 235–241, https://doi.org/10.1016/j.vacuum.2011.06.011.

46. C. P. Scott and P. A. Higham, "Antibiotic Bone Cement for the Treatment of Pseudomonas aeruginosa in Joint Arthroplasty: Comparison of Tobramycin and Gentamicin-Loaded Cements," *Journal of Biomedical Materials Research Part B, Applied Biomaterials* 64, no. 2 (2003): 94–98, https://doi.org/10.1002/jbm.b.10515.

47. C. Mollea, F. Bosco, and D. Fissore, "Agar Plate Methods for Assessing the Antibacterial Activity of Thyme and Oregano Essential Oils Against *S. epidermidis* and *E. coli*," *Antibiotics* 11, no. 12 (2022): 1809, https://doi.org/10.3390/antibiotics11121809.

48. N.-H. Chen, C.-J. Chung, C.-C. Chiang, K.-C. Chen, and J.-L. He, "Antimicrobial and Decorative Ion-Plated Copper-Containing Ceramic Coatings," *Surface & Coatings Technology* 236 (2013): 29–35, https://doi.org/10.1016/j.surfcoat.2013.04.012.

49. J. Osés, G. G. Fuentes, J. F. Palacio, J. Esparza, J. A. García, and R. Rodríguez, "Antibacterial Functionalization of PVD Coatings on Ceramics," *Coatings* 8, no. 5 (2018): 197, https://doi.org/10.3390/coatings8050197.

50. G. Zou and J. Bao, "Preparation and Antibacterial Properties of Porous Alumina Ceramics Coated With Silver Nanoparticles," *Materials Letters* 392 (2025): 138531, https://doi.org/10.1016/j.matlet.2025.138531.

51. Y. Zhang, X. Zhao, S. Fu, et al., "Preparation and Antibacterial Activity of Ag/TiO_2-Functionalized Ceramic Tiles," *Ceramics International* 48, no. 4 (2022): 4897–4903, https://doi.org/10.1016/j.ceramint.2021.11.026.

52. L. Wang, C. Hu, and L. Shao, "The Antimicrobial Activity of Nanoparticles: Present Situation and Prospects for the Future," *International Journal of Nanomedicine* 12 (2017): 1227–1249, https://doi.org/10.2147/IJN.S121956.

53. A. Ahmad, Y. Wei, F. Syed, et al., "The Effects of Bacteria-Nanoparticles Interface on the Antibacterial Activity of Green Synthesized Silver Nanoparticles," *Microbial Pathogenesis* 102 (2017): 133–142, https://doi.org/10.1016/j.micpath.2016.11.030.

54. A. Salleh, R. Naomi, N. D. Utami, et al., "The Potential of Silver Nanoparticles for Antiviral and Antibacterial Applications: A Mechanism of Action," *Nanomaterials* 10, no. 8 (2020): 1566, https://doi.org/10.3390/nano10081566.

55. E. O. Mikhailova, "Silver Nanoparticles: Mechanism of Action and Probable Bio-Application," *Journal of Functional Biomaterials* 11, no. 4 (2020): 84, https://doi.org/10.3390/jfb11040084.

56. D. Acharya, B. Mohanta, P. Pandey, and F. Nasiri, "Antibacterial Properties of Synthesized Ag and Ag@SiO_2 Core–Shell Nanoparticles: A Comparative Study," *Canadian Journal of Physics* 96, no. 8 (2018): 955–960, https://doi.org/10.1139/cjp-2017-0614.

57. Y.-S. Ko, Y. H. Joe, M. Seo, K. Lim, J. Hwang, and K. Woo, "Prompt and Synergistic Antibacterial Activity of Silver Nanoparticle-Decorated Silica Hybrid Particles on Air Filtration," *Journal of Materials Chemistry B* 2, no. 39 (2014): 6714–6722, https://doi.org/10.1039/C4TB01068J.

58. N. R. Rossi, B. Rossi Canuto de Menezes, A. da Graça Sampaio, et al., "Silver-Coated Silica Nanoparticles Modified With MPS: Potential Antimicrobial Biomaterials Applied in Glaze and Soft Reliner," *Polymers* 14, no. 20 (2022): 4306, https://doi.org/10.3390/polym14204306.

59. D. Sredojević, V. Lazić, A. Pirković, et al., "Toxicity of Silver Nanoparticles Supported by Surface-Modified Zirconium Dioxide With Dihydroquercetin," *Nanomaterials* 12, no. 18 (September 2022): 3195, https://doi.org/10.3390/nano12183195.

60. A. C. da Silva Rocha, M. V. Dos Santos Pinheiro, L. R. de Menezes, and E. O. da Silva, "Core-Shell Nanoparticles Based on Zirconia Covered With Silver as an Advantageous Perspective for Obtaining Antimicrobial Nanocomposites With Good Mechanical Properties and Less Cytotoxicity," *Journal of the Mechanical Behavior of Biomedical Materials* 123 (2021): 104726, https://doi.org/10.1016/j.jmbbm.2021.104726.

61. S. Atasoy, A. Yavuz, K. Ozcan, et al., "The Fabrication of Silver/Zirconia Coatings: Characterization, Corrosion and Antibacterial Properties," *Ceramics International* 51, no. 22 Part A (2025): 35541–35555, https://doi.org/10.1016/j.ceramint.2025.05.276.

62. L. Reyes-Carmona, O. A. Sepúlveda-Robles, A. Almaguer-Flores, J. M. Bello-Lopez, C. Ramos-Vilchis, and S. E. Rodil, "Antimicrobial Activity of Silver-Copper Coating Against Aerosols Containing Surrogate respiratory Viruses and Bacteria," *PLoS ONE* 18, no. 12 (2023): e0294972, https://doi.org/10.1371/journal.pone.0294972.

63. Y. Song, Y. Lee, Y. Lee, et al., "Anti-Viral, Anti-Bacterial, but Non-Cytotoxic Nanocoating for Reusable Face Mask With Efficient Filtration, Breathability, and Robustness in Humid Environment," *Chemical Engineering Journal* 470 (2023): 144224, https://doi.org/10.1016/j.cej.2023.144224.

64. Y.-I. Kim, M.-W. Kim, S. An, A. L. Yarin, and S. S. Yoon, "Reusable Filters Augmented With Heating Microfibers for Antibacterial and Antiviral Sterilization," *ACS Applied Materials & Interfaces* 13, no. 1 (2021): 857–867, https://doi.org/10.1021/acsami.0c16471.

65. S. Han, J. Kim, Y. Lee, et al., "Transparent Air Filters With Active Thermal Sterilization," *Nano Letters* 22, no. 1 (2022): 524–532, https://doi.org/10.1021/acs.nanolett.1c02737.